Originally published in the Proceedings of SMTA International,
Rosemont, IL, September 27-October 1, 2015

Strategic Environmental Research and Development Program (SERDP) Nanoparticle enhanced conformal coating project: Coating modeling for tin whisker mitigation

S. McKeown, S. Meschter*; BAE Systems
P. Snugovsky, J. Kennedy, Z. Bagheri, J. Keeping; Celestica
J. Cho; Binghamton University
D. Edwards; Henkel LLC
K. Elsken; Covestro LLC
*Corresponding Author stephan.j.meschter@baesystems.com

ABSTRACT

In 2006, the European Union RoHS legislation prohibited the use of lead in many electronic systems. This has resulted in increased use of pure tin finishes and tin rich lead-free alloys in aerospace and defense electronic systems. While aerospace and defense are currently exempt from the RoHS legislation, these industries adapt or directly use many consumer parts and assemblies. Unfortunately, the tin rich materials in these consumer items have a higher short circuit risk due to tin whiskers than heritage tin-lead materials. The whisker shorting potential can be mitigated by applying conformal coatings traditionally used for moisture protection to electronic assemblies. However, tin nodules and odd-shaped eruptions can also form, which can rupture the coating and reduce moisture protection and whisker mitigation effectiveness. The application of conformal coating to the original "tin free" surface alters the surface, changing the whisker nucleation and growth characteristics. A combination of finite element, classical plate deflection and adhesion models have been developed to examine the critical pressure that a tin nodule/whisker can exert on a coating before rupture or delamination occur. Supporting experimental results reveal that a high strength high modulus polyurethane conformal coating can inhibit nodule/whisker formation provided the coating is sufficiently thick and well adhered to the tin.

Key words: Tin Whiskers, Lead Free, Mitigation, Conformal Coating

BACKGROUND

Tin whisker growth generally occurs when thin tin or tin rich alloys are under "compressive" stress. As shown in Figure 1, whisker growth can occur due to stress sources such as copper substrate intermetallic (IMC) growth, corrosion/oxidation, differences in coefficient of thermal expansion under thermal cycling conditions, and from mechanical loads [1]-[3]. While much of the reported whisker growth has been on tin plating, lead-free solder can also grow whiskers, particularly where it is less than 25 microns thick [4][5][7] (Figure 2). Equipment in harsh service conditions experiences thermal cycling, vibration, shock, humidity, salt fog, sulfur rich environments, rework, and long term storage, which can all contribute to whisker growth.

The formation of tin whiskers can result in short circuits which are difficult to find and cause unexpected system behavior [8]. The aerospace and defense electronic systems recognize the potential impact of tin whisker shorting and utilize multiple mitigations to reduce the risk. Mitigations include lower whisker propensity material combinations, barriers, spacing, conformal coating, and redundant system design [9].

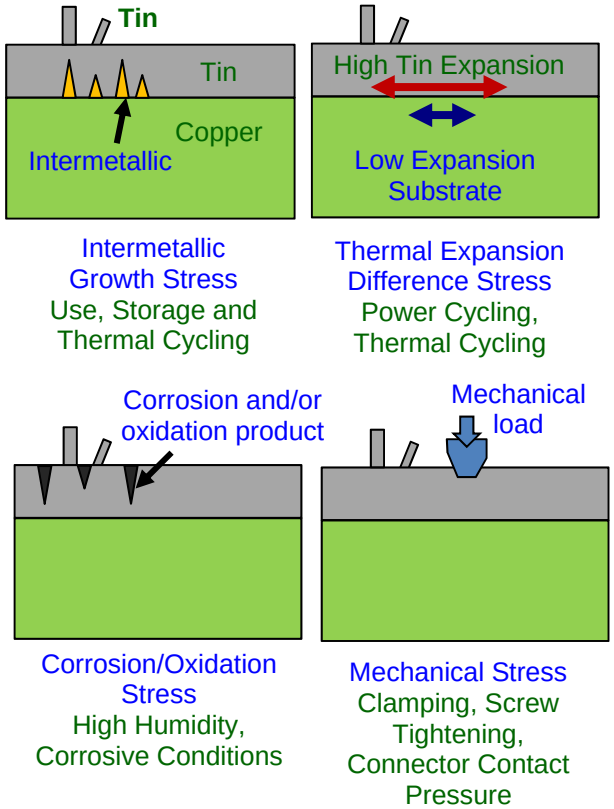

Figure 1: Some sources of compressive stress contributing to whisker growth.

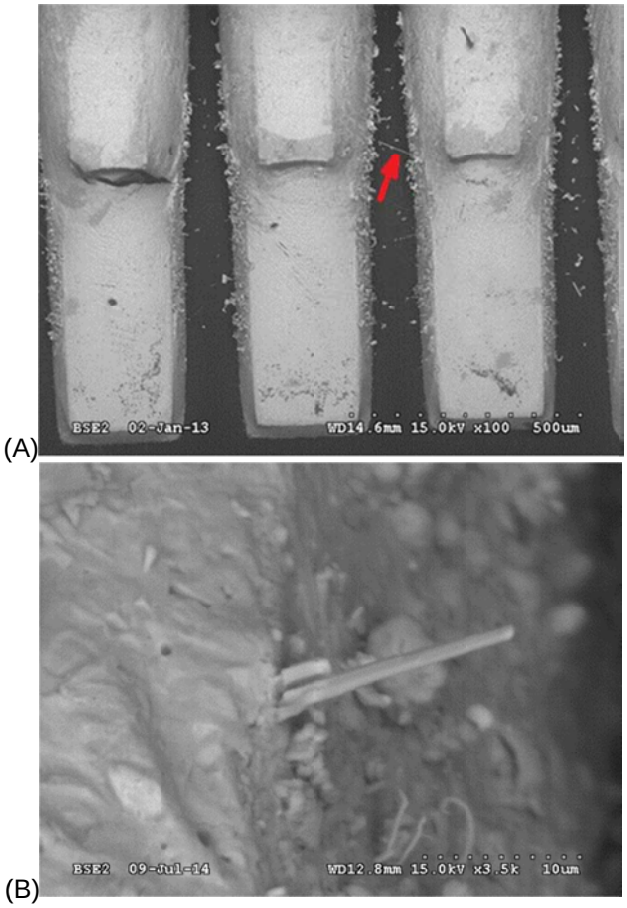

Figure 2: SEM images of corrosion/oxidation and whisker growth of Sn3Ag0.5Cu (wt%) soldered Cu alloy lead terminations to Cu board pads. (A) A 64 pin quad flat pack (cleaned part before assembly and cleaned after soldering) after 4,000 hours at 85ºC/85%RH. Arrow indicates a broken whisker that has nearly bridged between the printed wiring board pads, 100x [6]. (B) A SOT5 (cleaned part before assembly and low level NaCl contamination of 10 microgram/in^2 equivalent ionic contamination after assembly cleaning) exposed for 16,910 hours of 25ºC/85%RH, 3,500X [7].

Conformal coating is particularly appealing to high reliability electronics manufacturers because it has been used extensively to provide moisture protection in aerospace and defense electronic systems. Many coating types have been qualified [see IPC-CC-830, IPC Association Connecting Electronics Industries, Bannockburn, IL and MIL-I-46058, U.S. Department of Defense] and varying whisker mitigation effectiveness has been observed [10] – [19]. Coating provides mitigation of tin rich lead-free materials by reducing environmental attack, altering the tin whisker nucleation kinetics on the tin surface, capturing whiskers under the coating, preventing contact from adjacent surface whisker growth (Figure 3).

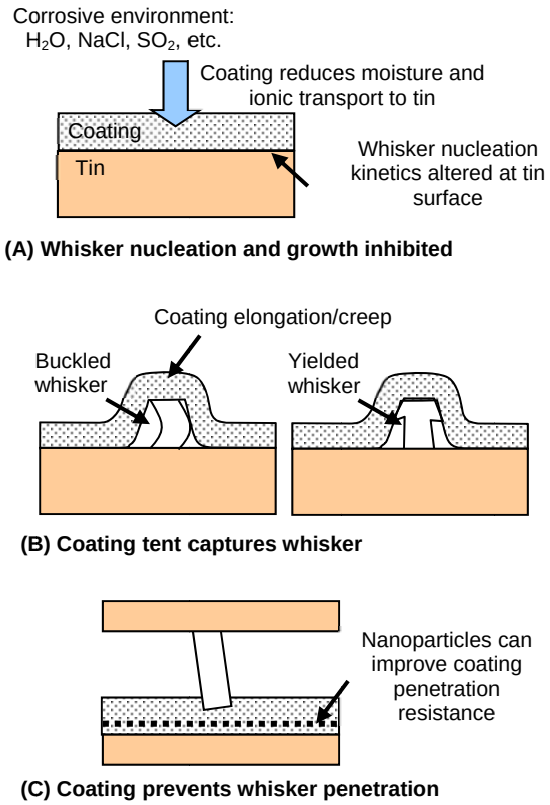

Figure 3: Coating whisker mitigation modes.

The results of coating whisker penetration resistance tests by several investigators found that Parylene ™ and urethane coatings exhibited better performance than acrylic and silicone coatings. In addition, thicker stronger coatings tended to exhibit a longer time before whisker penetration [10] – [19].

Some researchers have evaluated coating mitigation on actual electronic assemblies [10][18][19]. The assembly studies revealed that the coating coverage and thickness on actual electronic assemblies varies greatly. The most popular and economical coatings are liquid coatings applied with spray processes. Factors affecting the uniformity of a coating include application process parameters, the coating viscosity and wetting characteristics, and assembly geometry. Common observations are areas with no coverage (e.g. spray shadowed areas) or very thin coating (e.g. outside corners and vertical services influenced by surface tension and gravity thinning). These assembly observations have motivated an effort to understand the current coating coverage throughout the electronics industry [20] and efforts to develop enhanced coating properties and coverage [18].

One of the longest coating mitigation experiments has been underway at NASA Goddard [16] [17]. Tin plated brass substrates were coated with the soft and tough polyurethane, Arathane ™ 5750 (Formerly Uralane 5750). The coatings were not penetrated by whiskers over an 11 year period of office ambient testing as long as the

coatings were at least 50 microns thick. The researchers at NASA Goddard observed that the whiskers lifted and peeled the coating forming a tent until the whisker buckled or the coating failed. Some key aspects of conformal coating whisker mitigation modeling were given by Kadesch and Leidecker [16] (Figure 4).

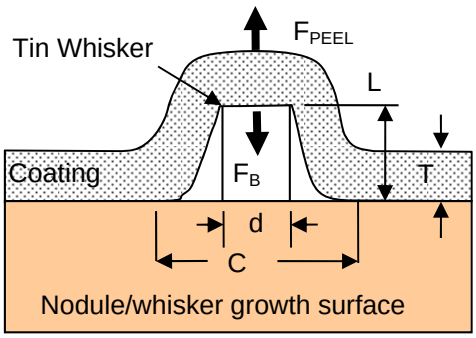

T = coating thickness
d = whisker diameter
L = whisker length
C = coating circumference peel ring

F_{PEEL} = coating peeling force
F_{TB} = whisker buckling force

Figure 4: Tin whisker buckling under coating.

COATING TIN WHISKER MITIGATION MODELING

The factors influencing tin nodule formation and/or tin nodule/whisker suppression under coating are not captured with a whisker buckling type of model. The development of a whisker or nodule under the coating causes pressure to be applied to the coating. The pressure application diameter could vary several orders of magnitude depending upon the type of tin growth. The diameter of a tin whisker can range from less than a micron to 20 microns. In the case of a nodule or an odd shaped eruption, the diameter can be on the order of 100 microns.

In this analysis, a combination of finite element, classical plate deflection and adhesion models are used to examine the critical pressure that a tin nodule/whisker can exert on a coating before rupture or delamination occur (Figure 5).

Coating analysis was based on three approaches:

A. Non-linear finite element analysis (FEA) to calculate the deflection in the coating to determine if the coating will rupture
B. Classical non-linear (plastic hinge) analysis to determine the deflection in the coating for comparison to the previous approach
C. Classical analysis to determine the energy release rate to delaminate the coating to determine in the coating will blister

Assumptions

The following assumptions were used in the analysis:

- The pressure exerted as a tin whisker develops is equal to the yield strength of tin
- Membrane deflection under pressure is neglected in the energy release rate calculations because the thinner coatings typically affected by membrane behavior would likely rupture and therefore not be influenced by delamination
- The outer boundary of the disk used in the energy release calculation is fixed initially but then limited to a critical bending moment value defined by plastic hinge behavior
- Yielding for the plastic hinge is elastic/perfectly plastic

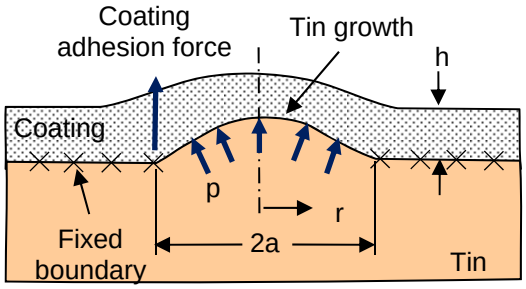

Figure 5: Schematic diagram of tin growth forming a dome in the coating.

Symbols and nomenclature

a = Outer Radius of Whisker/Radius of Applied Pressure
r = Variable Radius
E = Modulus of Elasticity
ν = Poisson's Ratio
h = Coating Thickness
w = Deflection (subscripts described in text)
M_a , M_{crit} = Moment at Radius a, Critical Plastic Hinge Moment
p = Pressure Applied from Whisker
p_{crit} = Critical Whisker Pressure
σ_r, σ_θ = Radial, Circumferential Stress
σ_1, σ_2, σ_3 = Principal Stresses
σ_{vm} = Von Mises Stress
σ_{crit} = Critical Stress
τ_{rv} = Radial-vertical Shear Stress
K_s = Shear Stress Effectiveness Factor
K_m = Plastic Hinge Moment Factor
G = Energy Release Rate, Shear Modulus (temporary variable)

Analysis and Modeling

The analysis is based on applying pressure in a circular area to represent the nascent tin whisker in a method similar to that used by B.T. Han [22] using the yield strength of tin (11 MPa [23]) as the applied pressure. Coating data was based on measurements by Cho [12] simplified into a bilinear curve (see Figure 6). The numerical value of the elastic modulus for coating below

the yield point was 500 MPa; the yield stress was taken as 34.5 MPa, and the tangent modulus as 7.29 MPa. The Poisson's ratio for the coating was estimated as 0.4999 based on the "rubbery" nature of the material and to attempt to maximize the indentation stiffness based on high measured hardness values.

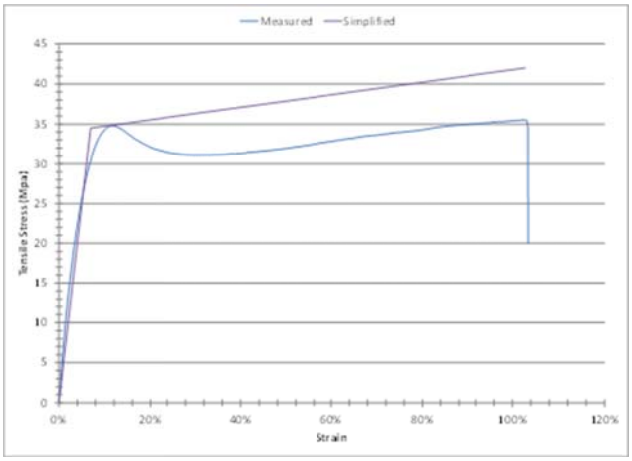

Figure 6: Coating Tensile Data Simplified Model.

A. Coating FEA to Determine Coating Deflection

The coating was modeled using axisymmetric 8-node rectangular parabolic elements using approximately 30,713 nodes and 10,080 elements (see Figure 7). The actual node and element count varied based upon the specific geometry which was automatically generated based on dimensions using an ANSYS macro. Symmetry constraints were applied along the left boundary (centerline), the right boundary was fixed, and pressure was applied to the lower surface (red arrow) to represent the action of the tin "nodule/whisker" (see Figure 8). The analysis was conducted for nodule/whisker diameters of 15, 30, and 45 microns and coating thicknesses of three and seven microns. Because the coating properties were nonlinear, an iterative solution was required.

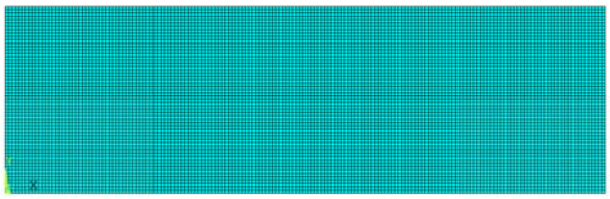

Figure 7: Finite element model (Diam. = 45 µm, Thick. = 7 µm)

Figure 8: Model boundary conditions

B. Classical Deflection Calculations

Coating deflection was determined analytically by considering the coating as an axisymmetric disk with both shear and bending deflection included. Bending deflection relationships included a bending moment applied along the outer edge to allow consideration of a plastic hinge. A plastic hinge is a consideration for beams in bending where the bending stress is considered to increase up to the yield stress and then remain constant at the yield stress, e.g. elastic-perfectly plastic, (see Figure 9). Once the cross-section is fully yielded (half in compression and half in tension at yield stress), the beam is considered a plastic hinge allowing unlimited bending rotation at a critical moment. The critical moment for a rectangular cross-section is 1.5 times the moment where yielding begins.

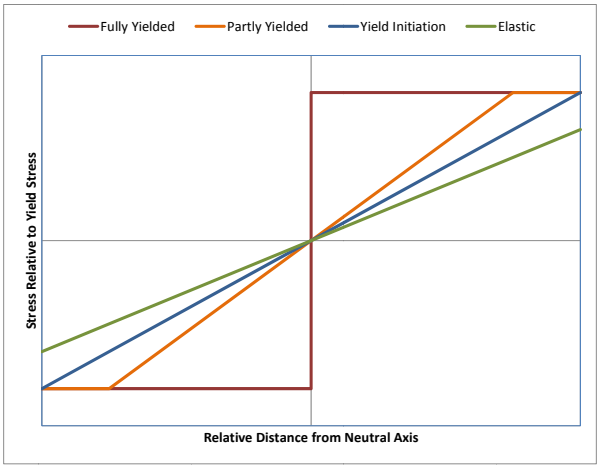

Figure 9: Plastic hinge stress versus position.

Bending deflection for a disk with uniform pressure and a variable edge moment is given by the following equations:

General Deflection due to bending:

$$w_b = \frac{\left(a^2 - r^2\right)\cdot\left[(\nu + 5)\cdot a^2 - r^2\cdot(\nu + 1)\right]}{64\cdot D\cdot(\nu + 1)}\cdot p + \frac{M_a\cdot\left(a^2 - r^2\right)}{2\cdot D\cdot(\nu + 1)}$$

Deflection at center (r = 0):

$$w_b = \frac{a^4\cdot(\nu + 5)}{64\cdot D\cdot(\nu + 1)}\cdot p + \frac{a^2 M_a}{2\cdot D\cdot(\nu + 1)}$$

Plate stiffness:

$$D = \frac{E\cdot h^3}{12\cdot\left(1 - \nu^2\right)}$$

Moment at edge for fixed edge (limited by plastic hinge):

$$M_a = -\frac{a^2\cdot p}{8}$$

The above equations correctly predict deflection for the simply supported case ($M_a = 0$) and the fixed edge case ($M_a = -a^2p/8$). When yielding occurs, the moment is limited by the plastic hinge effect described above.

Although the bending deflection equations produce good results for thin disks of coating, thicker coatings require consideration of shear deflection as follows:

General deflection due to shear:

$$w_s = \frac{p\cdot\left(a^2 - r^2\right)}{4\cdot G\cdot h}$$

Deflection at center (r = 0):

$$w_s = \frac{a^2\cdot p}{4\cdot G\cdot h}$$

Shear modulus:

$$G = \frac{E}{2\cdot(1+\nu)}$$

It should be noted that the above shear deflection equations produce results 2/3 of the values given by Volterra and Gaines [24] this is because the reference used the peak shear stress (1.5 times average) in the cross-section to calculate deflection but better agreement with finite-element results is obtained by using the average shear stress. Stresses due to bending at the outside edge of disk are given by the following relationships:

Radial stress:

$$\sigma_r = \frac{6\cdot M_a}{h^2}$$

Circumferential stress:

$$\sigma_\theta = \frac{\left[3\cdot a^2\cdot(1-\nu)\right]\cdot p + 24\cdot M_a}{4\cdot h^2}$$

Initial attempts at plastic hinge calculations using the above equations compared well to finite-element results for thin coatings but showed considerable divergence for thicker coatings. Including shear stress given by the following equation improved agreement:

Radial-vertical shear stress:

$$\tau_{rv} = \frac{K_s\cdot a\cdot p}{2\cdot h}$$

K_s in the above equation is the shear stress effectiveness factor, and represents the effectiveness of shear in the Von Mises stress calculations. Theoretically the shear stress in a rectangular cross-section varies from zero at the top and bottom edges (where bending stress is highest) to 1.5 times average shear stress at the centerline. Although shear has no effect on the maximum Von Mises stress when yielding first occurs (because shear stress is zero, shear becomes important as the region of yielding moves toward the center of the cross-section. The specific value of K_s is empirically derived from the critical pressure determined by finite-element analysis. The shear stress is combined with the radial stress to determine the principal stresses, which are in turn used to determine the Von Mises stress as follows:

$$\sigma_1 = \frac{\sigma_r}{2} + \sqrt{\left(\frac{\sigma_r}{2}\right)^2 + \tau_{rv}^2}$$

$$\sigma_2 = \frac{\sigma_r}{2} - \sqrt{\left(\frac{\sigma_r}{2}\right)^2 + \tau_{rv}^2}$$

$$\sigma_3 = \sigma_\theta$$

$$\sigma_3 = \frac{\left[3\cdot a^2\cdot(1-\nu)\right]\cdot p + 24\cdot M_a}{4\cdot h^2}$$

Substituting:

$$\sigma_3 = \frac{\left[3\cdot a^2\cdot(1-\nu)\right]\cdot p + 24\cdot M_a}{4\cdot h^2}$$

$$\sigma_2 = \frac{3\cdot M_a}{h^2} - \sqrt{\frac{K_s^2\cdot a^2}{4\cdot h^2}\cdot p^2 + \frac{9\cdot M_a^2}{h^4}}$$

$$\sigma_3 = \frac{\left[3\cdot a^2\cdot(1-\nu)\right]\cdot p + 24\cdot M_a}{4\cdot h^2}$$

Von Mises Stress:

$$2\cdot\sigma_{vm}^2 = \left(\sigma_1 - \sigma_2\right)^2 + \left(\sigma_1 - \sigma_3\right)^2 + \left(\sigma_2 - \sigma_3\right)^2$$

Substituting:

$$2\cdot\sigma_{vm}^2 = \left[\frac{3\cdot\left(3\cdot\nu^2 - 6\cdot\nu + 3\right)}{8\cdot h^4}\cdot a^4 + \frac{3\cdot K_s^2}{2\cdot h^2}\cdot a^2\right]\cdot p^2 - \frac{9\cdot M_a\cdot a^2\cdot(\nu-1)}{h^4}\cdot p + \frac{72\cdot M_a^2}{h^4}$$

Solving for M_a and using a critical stress for the Von Mises stress can derive a critical moment, which is used to establish the critical plastic hinge moment:

$$M_a = \left[\frac{a^2\cdot(\nu-1)}{16}\right]\cdot p - \frac{\sqrt{64\cdot h^4\cdot\sigma_{vm}^2 - p^2\cdot\left[a^4\cdot\left(27\cdot\nu^2 - 54\cdot\nu + 27\right) + 48\cdot K_s^2\cdot a^2\cdot h^2\right]}}{48}$$

$$M_{crit} = K_m\cdot M_a$$

$$\sigma_{vm} = \sigma_{crit}$$

$$M_{crit} = K_m\cdot\left[\left[\frac{a^2\cdot(\nu-1)}{16}\right]\cdot p - \frac{\sqrt{64\cdot h^4\cdot\sigma_{crit}^2 - p^2\cdot\left[a^4\cdot\left(27\cdot\nu^2 - 54\cdot\nu + 27\right) + 48\cdot K_s^2\cdot a^2\cdot h^2\right]}}{48}\right]$$

The K_m in the above equation represents the ratio between the plastic hinge moment and that at which yield initiates. Theoretically, for a rectangular cross section in pure bending with elastic-perfectly plastic material behavior this value is 1.5 but stress combinations and the specific stress-strain curve can cause some variation. The specific value of K_m is empirically derived from the deflection obtained by finite-element analysis. From the above equations, it can be seen that there is a critical pressure that results in an unstable (imaginary) result. This critical pressure is obtained by setting the relationship under the radical to zero and solving for pressure:

$$0 = 64\cdot h^4\cdot\sigma_{crit}^2 - p^2\cdot\left[a^4\cdot\left(27\cdot\nu^2 - 54\cdot\nu + 27\right) + 48\cdot K_s^2\cdot a^2\cdot h^2\right]$$

$$p_{crit} = \frac{8\cdot\sqrt{3}\cdot h^2\cdot\sigma_{crit}}{3\cdot a\cdot\sqrt{\left[9\cdot(\nu-1)^2\right]\cdot a^2 + 16\cdot K_s{}^2\cdot h^2}}$$

C. Energy Release Rate Calculations to Determine Coating Blistering

Energy release rate was determined by using the following steps by modeling the coating as an axisymmetric model of a disk:

1. Calculate the deflection of the coating in terms of thickness, radius, pressure, and material properties considering bending, shear, and bulk compression (membrane deflection is neglected as described in the assumptions)
2. Use the calculated deflection to determine the change in volume of the front surface of the coating and the energy absorbed by the coating
3. Differentiate the energy with respect to radius and divide by circumference to determine the energy release rate

C.1 Deflection Calculation

The bending deflection of a circular plate with radius=a fixed at the edge with a uniform pressure is given by [24]:

$$w = \frac{p\cdot a^4}{64\cdot D}\cdot\left(\frac{r^4}{a^4} - 2\cdot\frac{r^2}{a^2} + 1\right)$$

$$w_{max} = \frac{a^4\cdot p}{64\cdot D}$$

The shear deflection for a similar plate is given by:

$$w = \frac{p\cdot h^2}{24\cdot D}\cdot\frac{\left(a^2 - r^2\right)}{(1-\nu)}$$

$$w_{max} = \frac{a^2\cdot h^2\cdot p}{24\cdot D\cdot(1-\nu)}$$

The total deflection is obtained by summing the individual deflections and expressing the plate stiffness (D) in terms of the elastic modulus (E):

$$D = \frac{E\cdot h^3}{12\cdot\left(1-\nu^2\right)}$$

$$w = \frac{3\cdot p\cdot\left(a^2 - r^2\right)\cdot(1+\nu)}{4\cdot E\cdot h} + \frac{3\cdot p\cdot\left(a^2 - r^2\right)^2\cdot\left(1-\nu^2\right)}{24\cdot E\cdot h^3}$$

C.2 Volume Change and Energy Calculation

The volume change of the surface of the coating is determined by integrating the deflection over the radius as follows:

$$\Delta V = 2\cdot\pi\cdot\int_0^a\left[\frac{3\cdot p\cdot\left(a^2 - r^2\right)\cdot(1+\nu)}{4\cdot E\cdot h} + \frac{3\cdot p\cdot\left(a^2 - r^2\right)^2\cdot\left(1-\nu^2\right)}{24\cdot E\cdot h^3}\right]\cdot r\,dr$$

$$\Delta V = \frac{\pi\cdot a^4\cdot p\cdot(\nu+1)\cdot\left(a^2 - a^2\cdot\nu + 9\cdot h^2\right)}{24\cdot E\cdot h^3}$$

The coating energy is then calculated as follows:

$$U = \frac{p\cdot\Delta V}{2}$$

$$U = \frac{\pi\cdot a^4\cdot p^2\cdot(\nu+1)\cdot\left(a^2 - a^2\cdot\nu + 9\cdot h^2\right)}{48\cdot E\cdot h^3}$$

C.3 Energy Release Rate Calculation

The energy release rate is determined by differentiating with respect to the radius of the applied pressure (a) and dividing by the circumference as follows:

$$G = \frac{\frac{d}{da}U}{2\cdot\pi\,a} = \frac{\frac{\pi\cdot a^3\cdot p^2\cdot(\nu+1)\cdot\left(a^2 - a^2\cdot\nu + 6\cdot h^2\right)}{8\cdot E\cdot h^3}}{2\cdot\pi\cdot a}$$

$$G = \frac{a^2\cdot p^2\cdot(\nu+1)\cdot\left(a^2 - a^2\cdot\nu + 6\cdot h^2\right)}{16\cdot E\cdot h^3}$$

ANALYSIS RESULTS

Comparison of Classical and Finite-Element Deflection Calculations

Finite-element results were compared to the classical relationships described above for the coating thickness values and nodule diameters. Values of K_s and K_m were adjusted for best agreement on critical pressure and deflection respectively. These comparisons are plotted in Figure 10 and Figure 11.

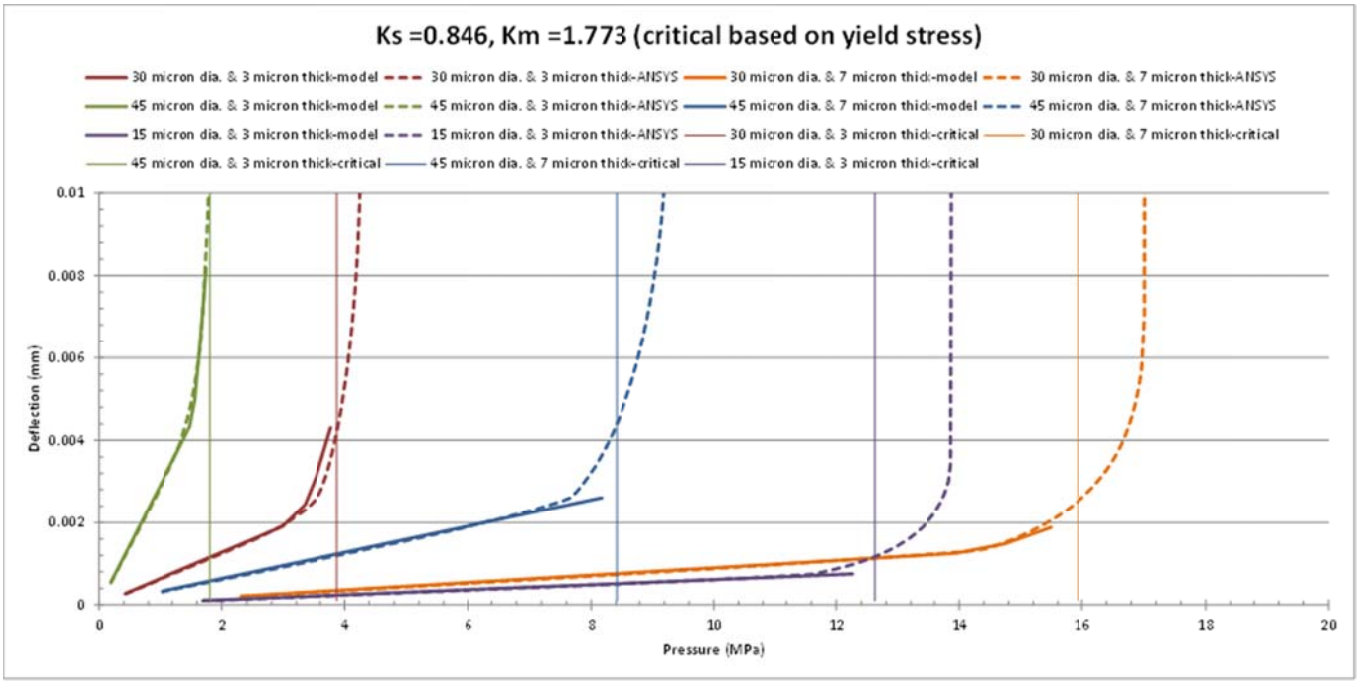

Figure 10 – Comparison of elastic/perfectly plastic FEA and classical models.

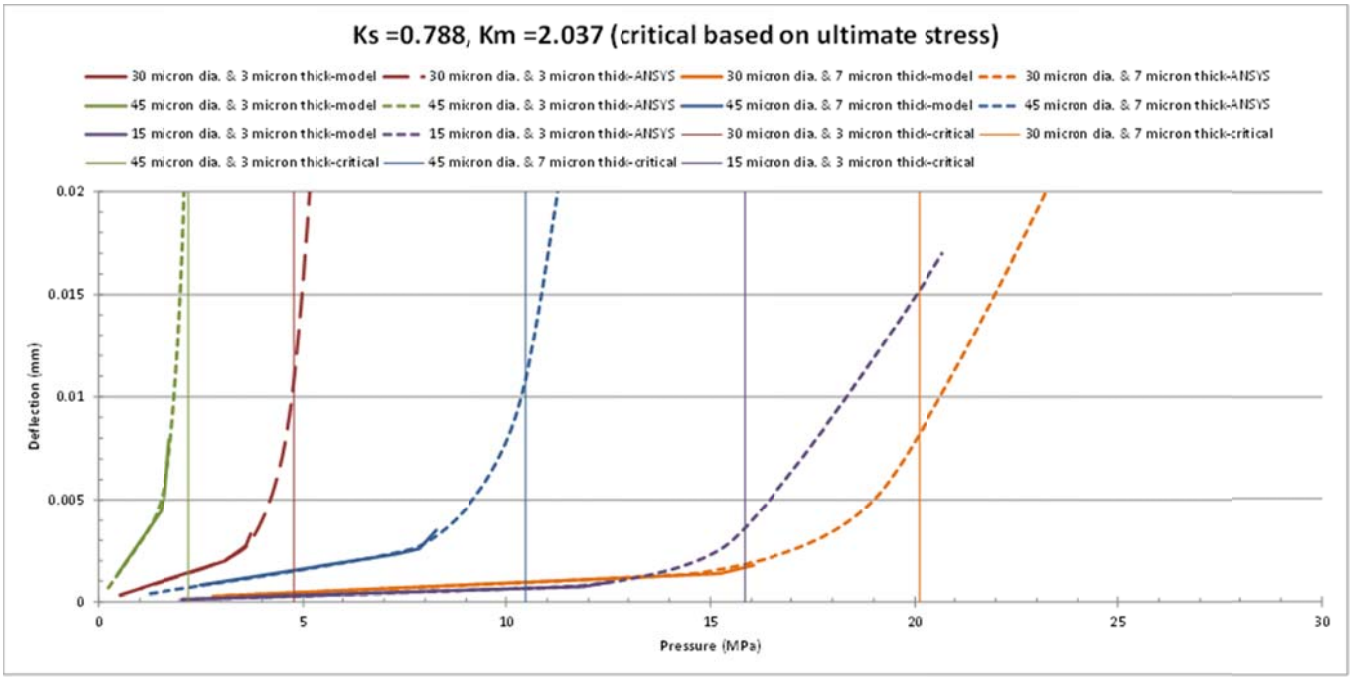

Figure 11: Comparison of maximum tensile at maximum elongation FEA and classical models

Analysis results for coating rupture

From the plots in the previous section, it is clear that there is a critical pressure where the coating deflection becomes unstable as confirmed by both classical and FEA. Analysis was conducted by solving the critical pressure equation for the critical stress to determine the minimum coating strength required for five different nodule/whisker diameters (up to 30 microns) as a function of thickness (see Figure 12). Here it can be seen that for a rubbery (ν = 0.4999) coating with a K_s value of 0.846 and a pressure of 11 MPa (tin yield strength), the coating will not fail with a coating thickness greater than 5.5 micron and a strength greater than 34.5 MPa for nodules less than 30 microns in diameter.

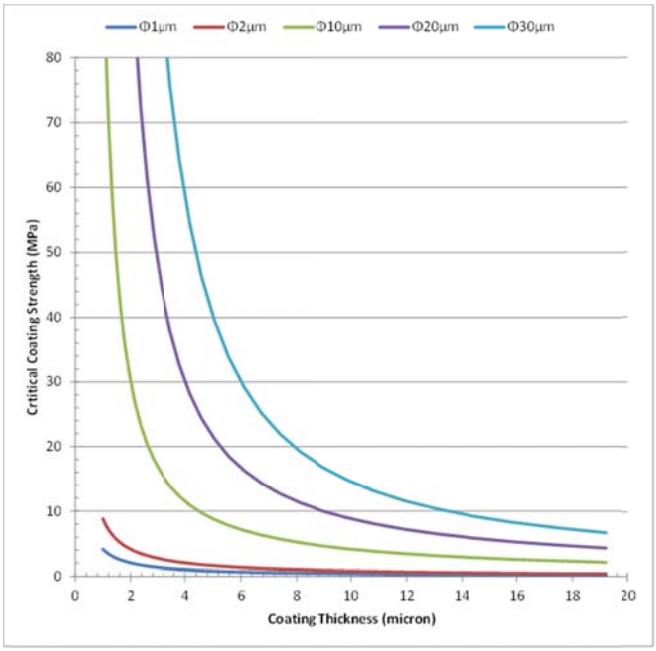

Figure 12: Critical coating strength required versus coating thickness

Energy Release Rate Calculation Results

Similar to the coating rupture approach, the minimum energy release rate is calculated for the same five nodule diameters (up to 30 microns) as a function of thickness (see Figure 13). Here it can be seen that for a rubbery (ν = 0.4999) coating with an elastic modulus of 500 MPa and a pressure of 11 MPa (tin yield strength), the coating will not delaminate with a coating thickness greater than 4.5 micron and the critical adhesion energy of polyurethane of 14-15 $\mu J/mm^2$ [21] for nodules less than 30 microns in diameter. (Note that the authors in [21] indicated that the 14-15 $\mu J/mm^2$ critical adhesion energy is a lower limit since during testing the interface between the epoxy and the polyurethane failed before the polyurethane to tin interface.)

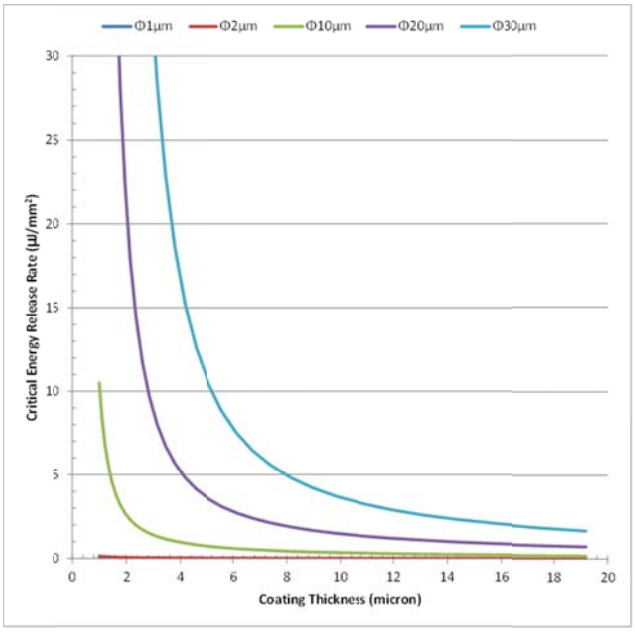

Figure 13: Critical energy release rate versus coating thickness

A SIMPLE EXPERIMENT

An initial experiment was performed to evaluate the whisker mitigation effectiveness of a nanosilica particle re-enforced polyurethane conformal coatings with enhanced strength. The coating formulation [11][12] and tin whisker growth experimental [18] details have been described in these references and key points will briefly be summarized next.

Coating Formulation

The conformal coating was prepared by mixing polyurethane resin with a nanoparticle suspension. The polyurethane resin system was chosen because it can be formulated to have a wide range of liquid viscosity and solid physical properties. Moisture curable solvent-based polyurethane (modified PC18M, from Henkel) was used in this formulation. The silica nanoparticles were dispersed in a hexamethylene diisocyanate (HDI) system (Desmodur® XP2742, from Covestro (formerly Bayer MaterialScience)) that is chemically compatible with the base polyurethane systems. The nanoparticles in the suspension were functionalized with an isocyanate to crosslink with the polymer chains in the base system. High-speed dispersion or sonication was employed to facilitate particle dispersion in the suspension medium. The present whisker coupon work used the PC18M+30%XP2742 (9.75wt% nanosilica) coating because it had the highest elastic modulus and tensile strength of the compositions tested (See Appendix A).

Cantilever beam whisker coupon

The cantilever beam coupon had bright tin plating over C110 alloy copper (see Figure 14). The plating was specified to be five to eight microns thick but was actually received at 20 microns which is above the optimal thickness for whisker growth. Note that a bright tin plated

C110 alloy also was used in other long-term tests [13] [14] in an effort to evaluate slower more realistic whisker growth than the bright tin over brass coupons [15][16][17]. The tin plated copper cantilever beam coupons were solvent cleaned and then draw coated with PC18M+30%XP2742 using shims and a doctor blade to obtain a final nominal thickness of 100 microns. After liquid coating application, the samples were air dried for a minimum of 30-45 minutes and then cured for a minimum of two hours at 60 ºC in an oven having a minimum relative humidity of 30 percent in accordance with the PC18M datasheet. After coating air drying, the tape was removed along two long edges of the coupon exposing uncoated tin plating. The coating was 100 microns thick in the center of sample and thinned to less than three microns near the internal beam edges.

The coupons were then installed in an aluminum fixture that clamped one end and raised the other end. The 0.38 mm free end displacement resulted in a bending preload of 11.4 MPa near the clamp.

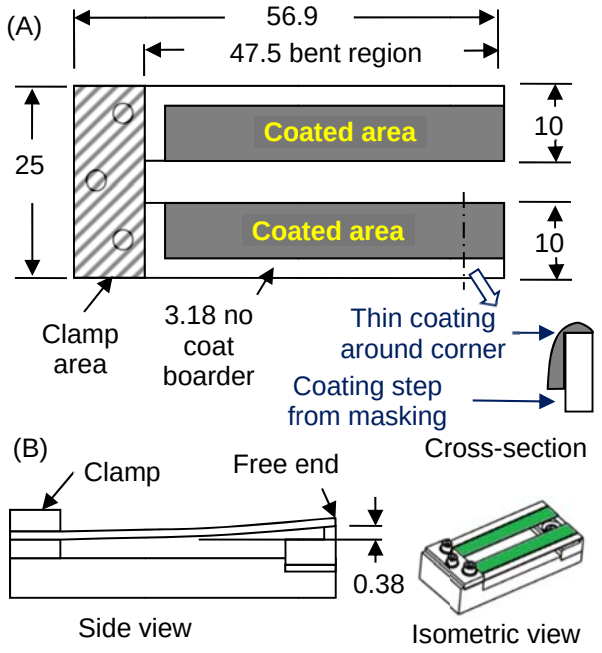

Figure 14: Cantilever beam whisker coupon; (A) coated cantilever beam, and (B) cantilever beam installed in fixture. Dimensions in mm.

Whisker coupon environmental exposure and inspection results

Optical inspection up to 100x, scanning electron microscope (SEM) inspection up to 2,000x and metallurgical cross-sectioning were used to evaluate the sample.

The coated coupon was initially placed in 60°C/60%RH for 500 hours and inspected. There were small whiskers and nodules on the non-coated areas and no whiskers or nodules under the coating. The sample was returned to the humidity environment for a total of 2,500 hours (500+2,000 hours).

SEM examination at this point showed that the non-coated areas grew whiskers and nodules but that the adjacent 100 micron thick coated areas had no odd shaped eruption nodules or whisker growth (see Figure 15). However, where the coating was thin (~three microns), odd shaped eruptions broke through the coating; and when the coating was a little thicker (~seven to 30 microns), there was evidence of nodule formation under the coating (see Figure 16).

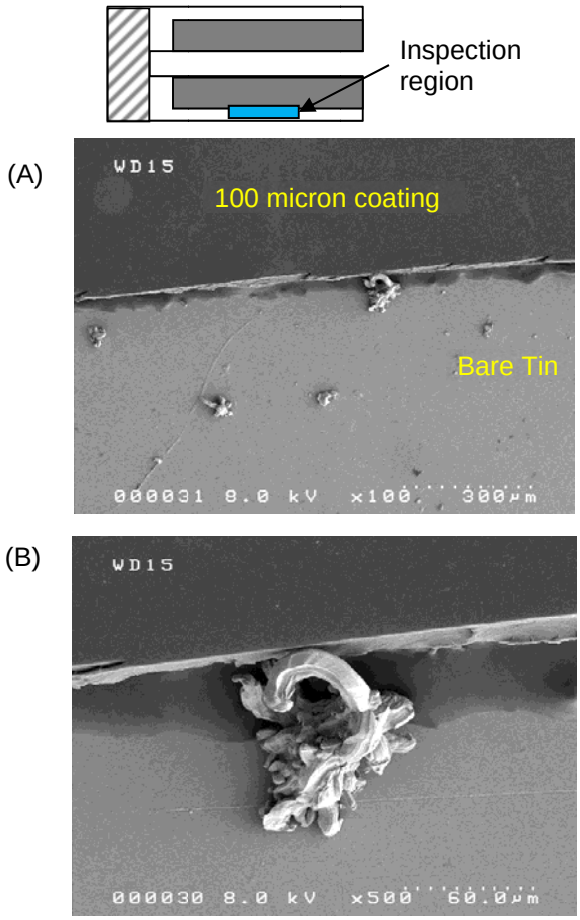

Figure 15: Cantilever beam coupon whisker growth from bare tin plating adjacent to the PC18M+30%XP2742 coating step areas after 2,500 (500+2,000) hours 60°C/60%RH; (A) overall and (B) high magnification image of nodule and whisker.

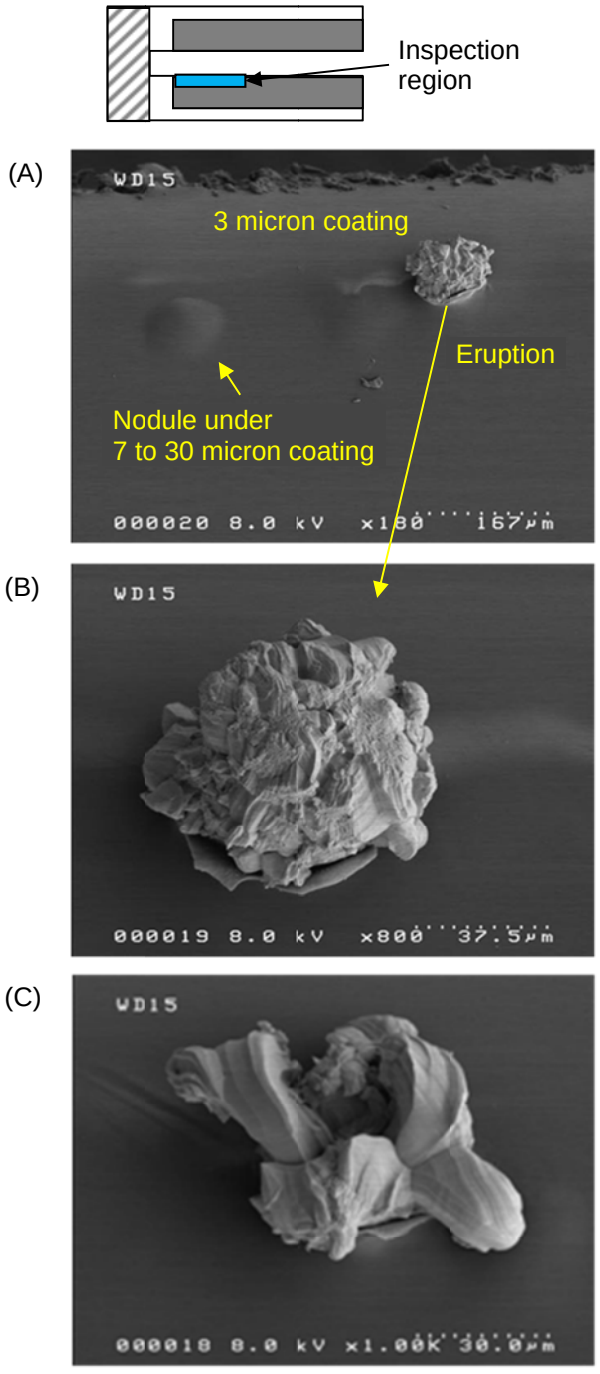

Figure 16: Cantilever beam coupon nodule growth; (A) overall, (B) and (C) close up of eruptions through thin coating.

Examination of the tin under the coating is inherently difficult, however it is possible to see through the coating optically with limited magnification. The scanning electron beam can only inspect the top surface of the coating. To evaluate the "absence of whisker nodules" under the thick coating regions, the coating was removed on the upper leg of the cantilever beam with Uresolve™ solvent. It was found that the 100 micron thick coating significantly inhibited nodule eruptions and whisker growth (Figure 17).

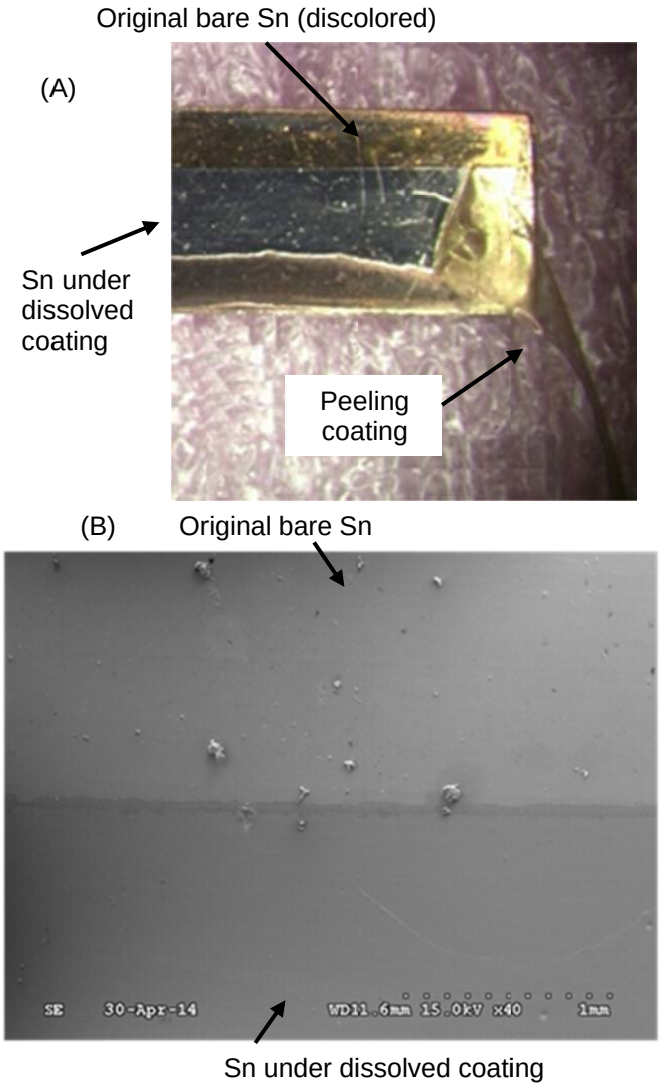

Figure 17: Cantilever beam coupon coating removal; (A) sample during dissolution process and (B) SEM inspection after coating removal.

Close inspection of the Sn area under the dissolved coating revealed evidence of possible small adhesion defects (Figure 18) and a possibly a small smooth nodule (Figure 19).

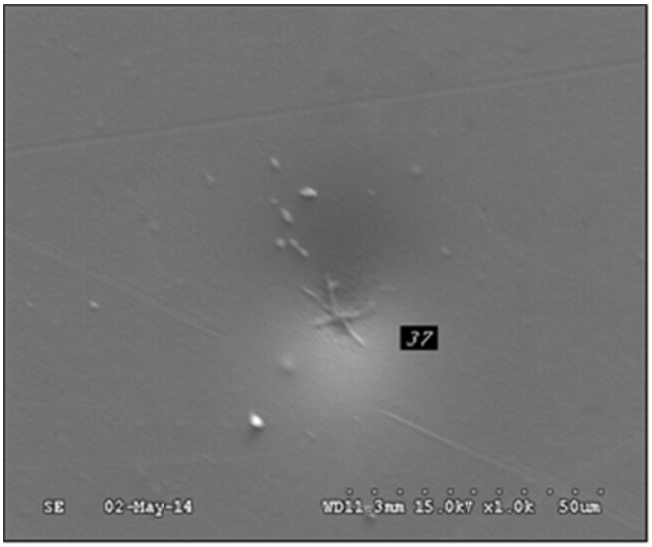

Figure 18: Possible adhesion defect between the coating and the tin.

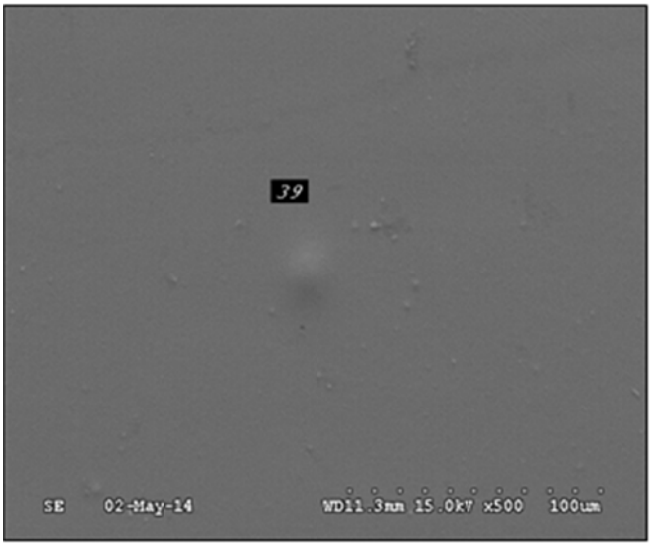

Figure 19: Possible nodule under coating.

The tin eruptions through the coating and nodules under the thinner coating, similar to those shown in Figure 16, were cross-sectioned to verify that these were in fact nodules and not debris captured under the coating during processing. The cross-sections verified that the nodules were tin dome-like structures. The tin dome diameter was smaller when the coating was thinner (Figure 20).

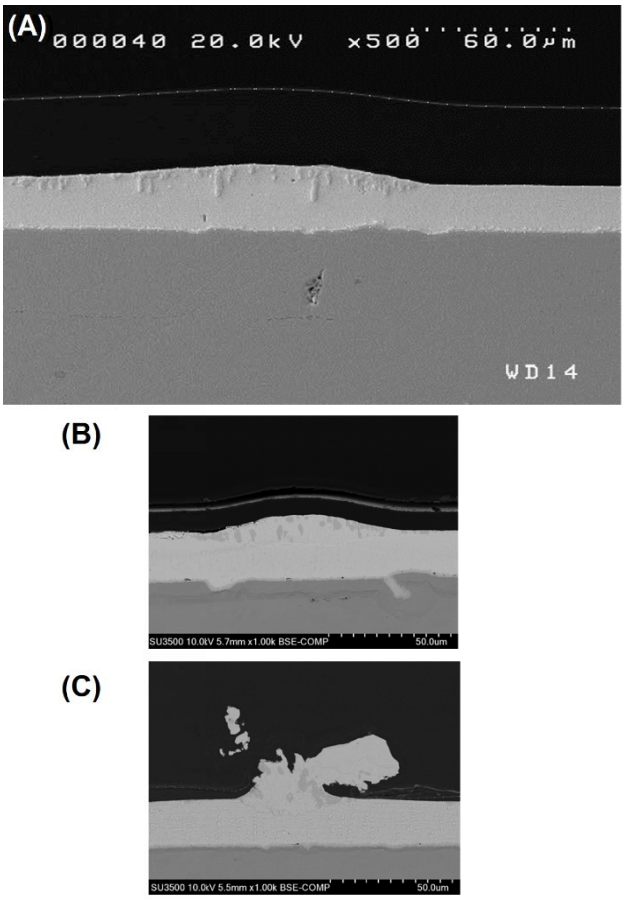

Figure 20: Cantilever beam coupon longitudinal cross-section through thin coating region. Comparison images at the same scale of the (A) 30 micron, (B) seven micron, and (C) three micron thick coating regions.

Ion beam polishing was used to obtain enhanced images of the nodules (Figure 21 and Figure 22). The curvature change between the flat tin surface and the beginning of the nodule is an area that is susceptible to delamination (Figure 21).

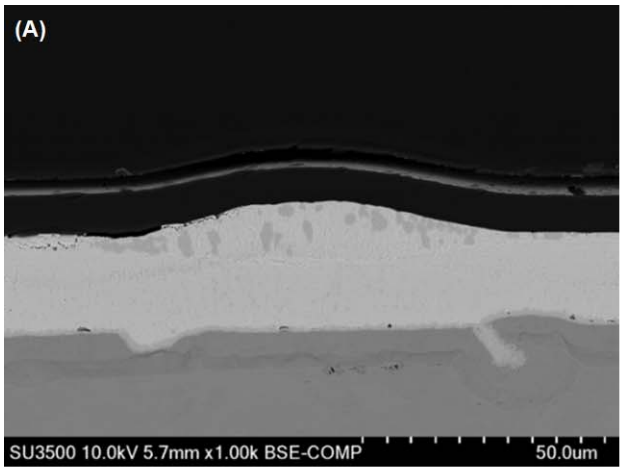

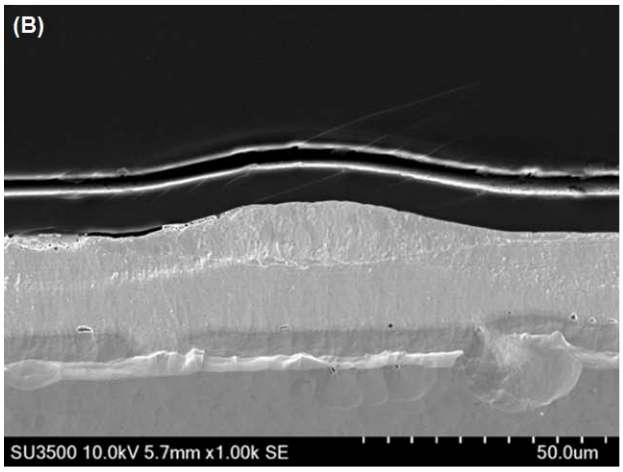

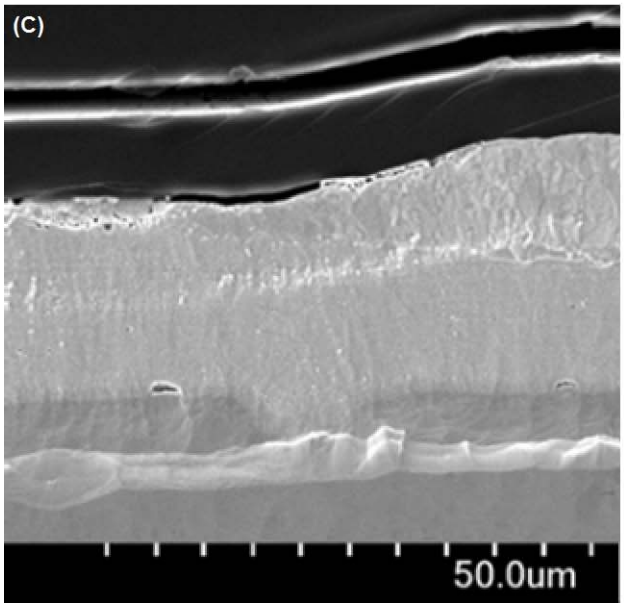

Figure 21: Ion beam polished section of the eruption through the seven micron coating: (A) back scatter electron image, (B) secondary electron image, and (C) close up of left side of dome showing coating delamination from the tin. (Note: the top most light lines in images B and C highlight a separation between the section potting material and the coating.)

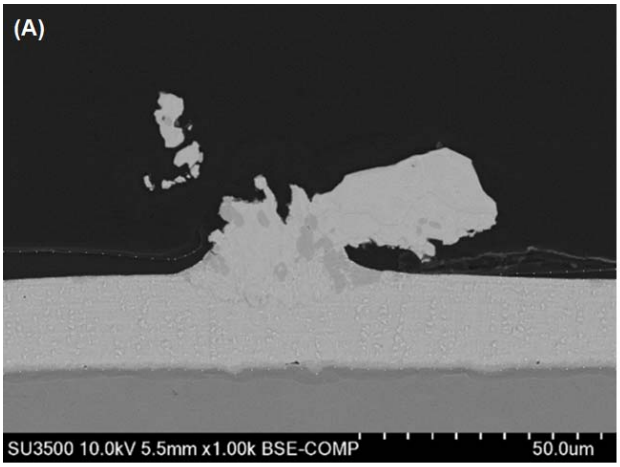

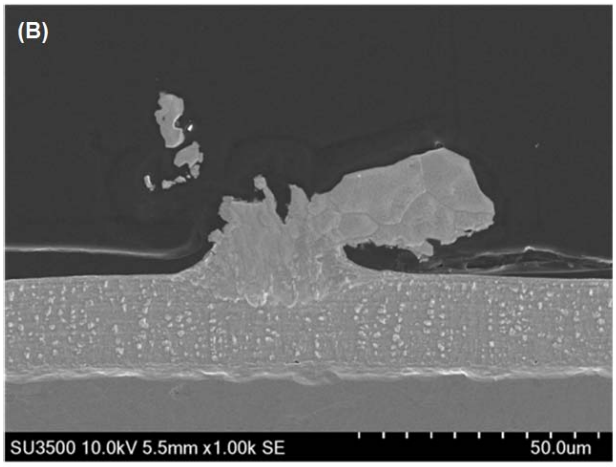

Figure 22: Ion beam polished section of the eruption through the three micron coating: (A) back scatter electron image, and (B) secondary electron image.

Measurements were obtained from the three nodule cross-sections to determine the nodule geometry and coating thickness profile. The dome heights were observed to be similar for the seven and 30 micron thick coating regions, but the diameters increased with increasing coating thickness (Figure 23). The coating typically thinned slightly near the apex of the tin dome (Figure 24). A summary of coating thicknesses and the tin dome diameter and height are given in Table 1.

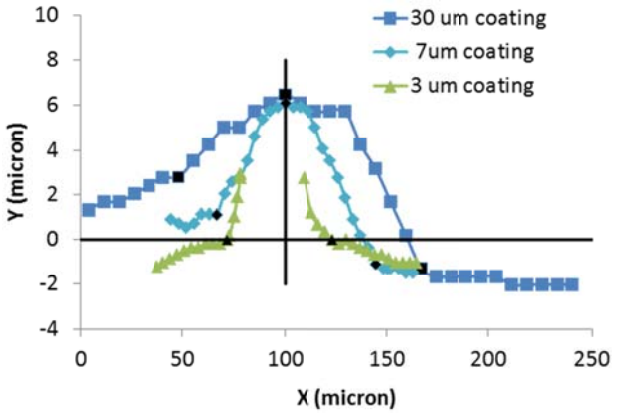

Figure 23: Measured tin dome height profiles for various coating thickness regions on the cantilever beam whisker test sample.

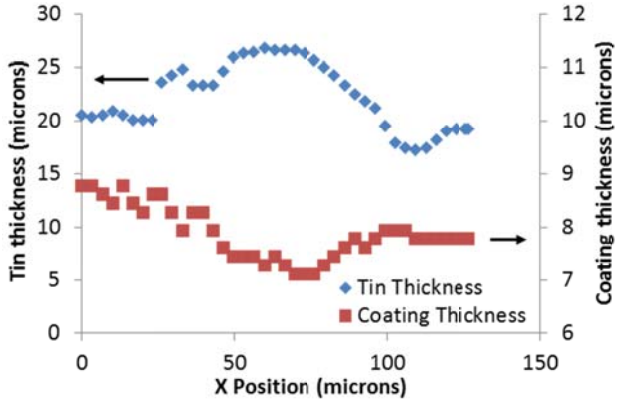

Figure 24: Typical measured tin and coating thickness values across the sample. The second ion beam mill section measurements from the seven micron thick coating shown.

Table 1: Coating thickness and tin dome measurement summary.

Nominal coating thickness	Average coating thickness in flat region (microns)	Minimum coating thickness at top of dome (microns)	Dome diameter (microns)	Dome height (microns)
3 um	3.4	Ruptured	51.6	Ruptured
7 um	8.2	7.1	79.5	6.8
30 um	30.2	28.5	118.5	5.7

DISCUSSION

The nucleation inhibition observed with the rigid coating in the present work is in contrast to the behavior of the softer Arathane 5750, where nodule nucleation of bright tin over brass under the coating was much greater than the uncoated areas [16]. The authors reported that at four months of exposure at 50°C, the coated side of the coupons exhibited four to five times more nodule and whisker growth than the uncoated side. However after a year, the density of growth on the non-coated side increased rapidly and was similar to the coated side. The authors also noted that a number of tin nodules appeared to be on the verge of breaking through the thinner regions of the coating, with the tin domes developing sharper tips over time.

In the present experiments, the coatings were considerably more rigid than the Arathane ™ 5750 (see Figure 25 and Figure 26. Although the PC18M+XP2742 properties are reduced at temperatures above the PC18M glass transition temperature, they are still higher than the Arathane (Figure 27).

Since whisker growth is a surface stress relaxation phenomena causing formation of the tin filament structure, it is reasonable that the presence of the rigid coating on the tin surface could inhibit whisker nucleation. However, conformal coating can negatively impact the solder thermal cycling reliability if not implemented properly [25][26].

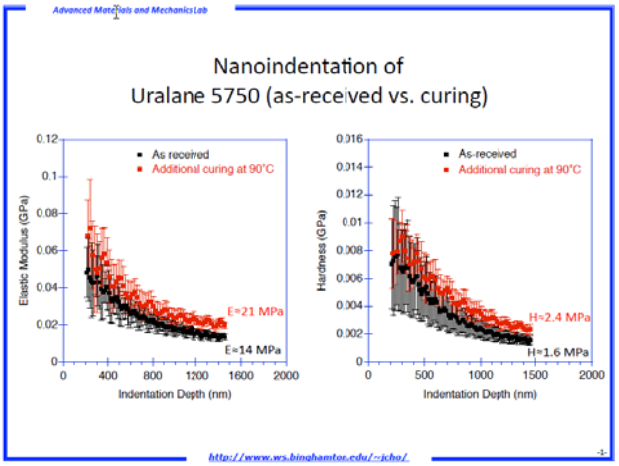

Figure 25: Nanoidentation of Arathane 5750 on a glass slide. The as-received measurements were obtained after the initial cure of 6 hours at 85 °C. The measurements were repeated after an additional exposure of 10 hours at 90°C.

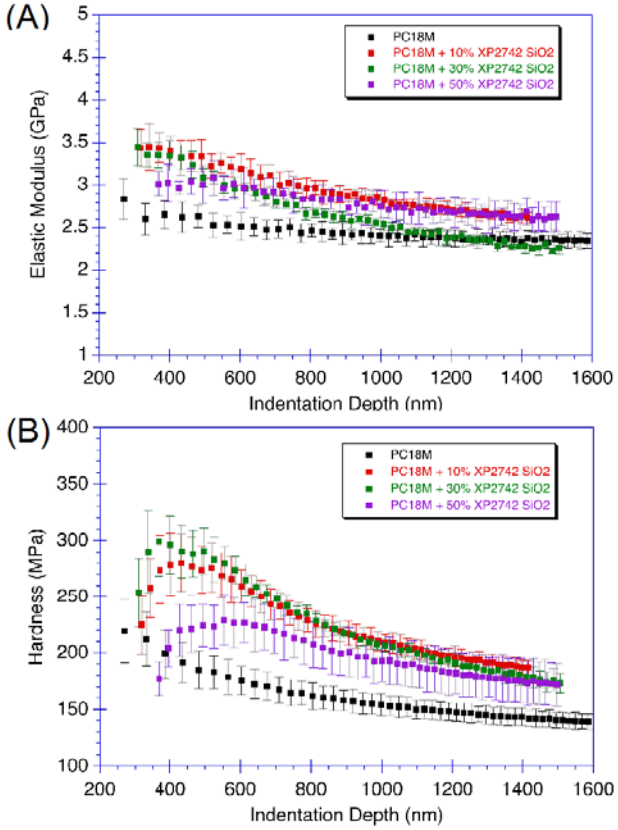

Figure 26: Nanoindentation testing results of PC18M filled with XP2742 (nanosilica); (A) elastic modulus, and (B) nanohardness.

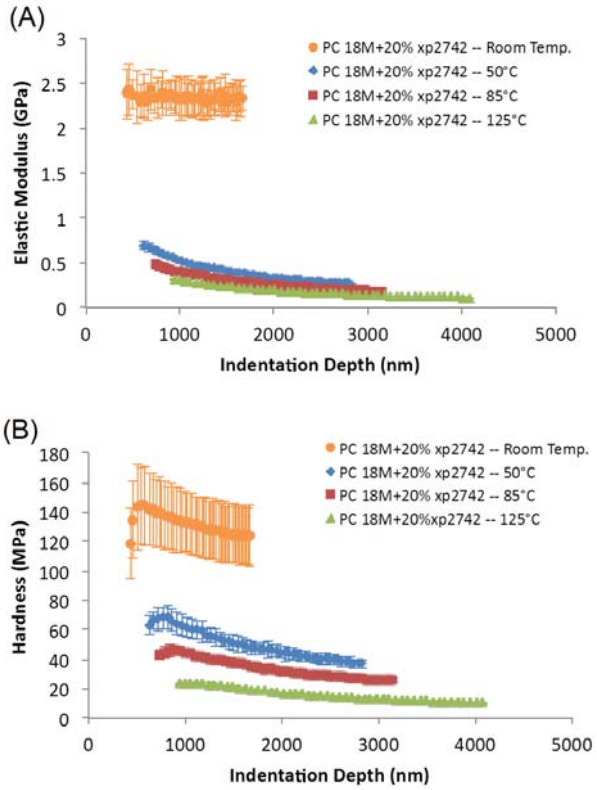

Figure 27: Nanoindentation testing results of PC18M+20% XP2742 at room temperature, 50˚C, 85˚C, and 125˚C; (a) elastic modulus, and (b) nanohardness.

SUMMARY

The modeling showed reasonable correlation with the experimental whisker coupon results. The FEA modeling predicted rupture of a three micron thick coating which was consistent with the rigid coating experimental observations. Energy release rate results also indicate that delamination of a 100 micron coating thickness is unlikely for typical whisker diameters.

If the nodule/whisker diameter was larger, the coating needed to be thicker and/or stronger to provide mitigation. Subsequently whiskers could grow through the rupture site. In addition, the rupture area could have increased tin corrosion and/or electrical leakage.

CONCLUSIONS

The following conclusions can be made

- There is a combination of coating thickness, strength and adhesion that can provide whisker mitigation
- In contrast to smaller diameter whiskers, larger diameter tin nodule formations have greater potential to rupture the coating
- The whisker growth surface stress relaxation phenomena causing formation of the tin filament structure is altered in the presence of a coating having high adhesion, high strength, and sufficient thickness
- Although rigid coatings can inhibit tin nodule/whisker formation they need to be evaluated for potential impacts to solder joint thermal cycling fatigue reliability

FUTURE OPPORTUNITIES

Further tests to provide correlation between coating blister size, coating thickness and coating strength/modulus are recommended. In addition, coating deformation under the very slow strain rates associated with tin whisker growth needs to be understood further. Further work is also needed to rapidly and reliably determine the coating mechanical properties, critical adhesion energy between coatings and whisker prone metal surfaces. It would also be beneficial to have a better means to examine the nodule/whisker growth under the coating.

ACKNOWLEDGEMENTS

The authors wish to thank the Strategic Environmental Research and Development Program (SERDP) office for providing funding for this research.

REFERENCES

[1] JP002, *Current Tin Whiskers Theory and Mitigation Practices Guideline*, Joint JEDEC Solid State Technology Association/IPC Association Connecting Electronics Industries document, March 2006

[2] T. Shibutani, Q. Yu, M. Shiratori, M. Pecht, Pressure-induced tin whisker formation, Microelectronics Reliability Vol, 48 (2008) pp. 1033–1039

[3] G.T. Galyon, Annotated Tin Whisker Bibliography and Anthology, IEEE Trans. Packag. Manuf. Vol. 28, No. 1, January 2005, pp. 94-122.

[4] P. Snugovsky, S. Meschter, Z. Bagheri, E. Kosiba, M. Romansky, and J. Kennedy, Whisker Formation Induced by Component and Assembly Ionic Contamination, Journal of Electronic Materials, February 2012, Volume 41, Issue 2, pp 204-223 available for download at http://link.springer.com/content/pdf/10.1007%2Fs11664-011-1808-5.pdf

[5] S. Meschter, P. Snugovsky, Z. Bagheri, E. Kosiba, M. Romansky, J. Kennedy, L. Snugovsky, and D. Perovic, Whisker Formation on SAC305 Soldered Assemblies, JOM, vol. 66 no. 11, pp. 2320-2333, Nov. 2014 (DOI) 10.1007/s11837-014-1183-9

[6] S. Meschter, P. Snugovsky, J. Kennedy, Z. Bagheri, E. Kosiba, and A. Delhaise, SERDP Tin Whisker Testing and Modeling: High Temperature/High Humidity Conditions, SMTA International Conference on Soldering and Reliability, Toronto, Ontario, Canada; May 14-17, 2013.

[7] S. Meschter, E. Ekstrom, P. Snugovsky, .J. Kennedy, Z. Bagheri, and E. Kosiba, Strategic Environmental Research and Development Program (SERDP) Tin Whisker Testing and Modeling: Long Term Low Temperature High Humidity Testing, International Conference on Soldering and Reliability (ICSR 2015) Toronto, Ontario, Canada; May 19-21, 2015.

[8] B. Sood, M. Osterman and M. Pecht, Tin Whisker Analysis of Toyota's Electronic Throttle Controls, Circuit World, Vol. 37, No. 3, 2011, pp. 4–9

[9] GEIA-STD-0005-2, Standard for Mitigating the Effects of Tin Whiskers in Aerospace and High Performance Electronic Systems, SAE International, Warrendale, PA

[10] S. Han, S. Meschter, M. Osterman and M. Pecht, Evaluation of Effectiveness of Conformal Coatings as Tin Whisker Mitigation, Journal of Electronic Materials, DOI: 10.1007/s11664-012-2179-2, July 6, 2012.

[11] J. Cho, S. Meschter, S. Maganty, D. Starkey, M. Gomez, D. Edwards, A. Ekin, K. Elsken, J. Keeping, P. Snugovsky, and J. Kennedy, Characterization of Hybrid Conformal Coatings used for Mitigating Tin Whisker Growth, SMTA International Conference on Soldering and Reliability, Toronto, Ontario, Canada, May 14-17, 2013

[12] J. Cho, S. Meschter, S. Maganty, D. Starkey, M. Gomez, D. Edwards, A. Ekin, K. Elsken, J. Keeping, P. Snugovsky, J. Kennedy, and M. Romansky, Polyurethane Conformal Coatings Filled with Hard Nanoparticles for Tin Whisker Mitigation, SMTA International Conference on Soldering and Reliability, Toronto, Ontario, Canada, May 13-15, 2014.

[13] D. Hillman, Tin Whiskers Inorganic Coating Evaluation, 7th International Symposium on Tin Whiskers, Nov. 12-13, 2013, Costa Mesa, CA

[14] L. Woody and W. Fox, Tin Whisker Risk Management by Conformal Coating, SMT magazine, July 2014, pp. 40-58.

[15] T. Woodrow, E. Ledbury, Evaluation of Conformal Coatings as a Tin Whisker Mitigation Strategy, Part 2, Proceedings of the SMTA International Conference, September 24-28, 2006.

[16] J. Kadesch, H. Leidecker, Effects of Conformal Coat on Tin Whisker Growth, Proceedings of IMAPS Nordic, The 37th IMAPS Nordic Annual Conference, pp. 108-116, September, 10-13, 2000

[17] L. Panashchenko, J. Brusse and H. Leidecker, Long Term Investigation of Urethane Conformal Coating Against Tin Whisker Growth Tenting of 2mil conformal coating, IPC Tin Whisker Conference Dec. 7, 2010

[18] S. Meschter, J. Cho, S. Maganty, D. Starkey, M. Gomez, D. Edwards, A. Ekin, K. Elsken, J. Keeping, P. Snugovsky, and J. Kennedy, Nanoparticle Enhanced Conformal Coating for Whisker Mitigation, SMTA International, Sept/Oct 2014

[19] M. Wickham, K. Clayton, C. Hunt, and B. Dunn, Sn whiskers and their mitigation for space, aerospace and defence electronics, EMPPS 5th Electronic Materials, Processes and Packaging for Space (EMPPS) Workshop, Noordwijk, NL, 20-22 May 2014

[20] D. Hillman IPC J-STD-001 Committee 522 AAR Conformal Coating Material & Application Industry Assessment, IPC Pb-Free Electronic Risk Management Council Meeting (PERM 25) and SAE G24 Lead-free Document Committee Meeting, Dayton (Beavercreek), OH, July 21-23, 2015

[21] M. Roma, S. Maganty, R. Roeder, J. Cho, S. Meschter; “Evaluation of Interfacial Adhesion of Polyurethane Conformal Coatings Used for Tin Whisker Mitigation”; Materials Science and Technology 2014 Conference and Exhibition, October 12-16, 2014 Pittsburgh, PA

[22] B.T. Han, C. Jang, K. Mahan, S. Han, M. Osterman, Long Term Reliability Evaluation of Conformal Coatings for Tin Whisker Failure Mitigation, University of Maryland, 2010.

[23] matweb.com; “Tin, Sn”

[24] E. Volterra, and J, Gaines, Advanced Strength of Materials; Prentice Hall, 1971

[25] G. Caswell, C. Tulkoff and N. Blattau, The Effect of Coating and Potting on the Reliability of QFN Devices, DFR Solutions

[26] J. Wilcox, M. Meilunas and M. Anselm., Harsh Environment Reliability and Conformal Coat, SMTAi 2015

APPENDIX A: Nanoparticle enhanced polyurethane properties

In the present work, tensile testing on film samples was performed to provide macroscopic properties for modeling [12]. Testing was done at room temperature in accordance with ASTM D882 except the sample size was 63.5 x 12.7 mm (2.5 x 0.5 inch) with a gauge length of 12.7 mm (0.5 inch) and the displacement rate was 2.54 mm/minute (0.1 in/min). Ultimate tensile strength, yield strength, and modulus were obtained on PC18M (unfilled, PC18M+XP2472 (XP2742 has both nanosilica particles + N3300 isocyanate) and PC18M+N3300. The PC18M+N3300 isocyanate formulations were selected to separate the influences of the nanosilica and the N3300 isocyanate on the PC18M properties. The compositions of the PC18M+N3300 materials match the N3300 isocyanate in PC18M+XP2742 compositions without the nanosilica.

As shown in Figure 28, the PC18M+30%XP2742 (9.75wt% nanosilica) had the highest elastic modulus and tensile strength, almost double the unfilled PC18M. It should be noted that the PC18M+20%XP2742 (6.74 wt% nanosilica) composition was formulated to try to obtain better elongation and was eventually selected for assembly level whisker mitigation testing.

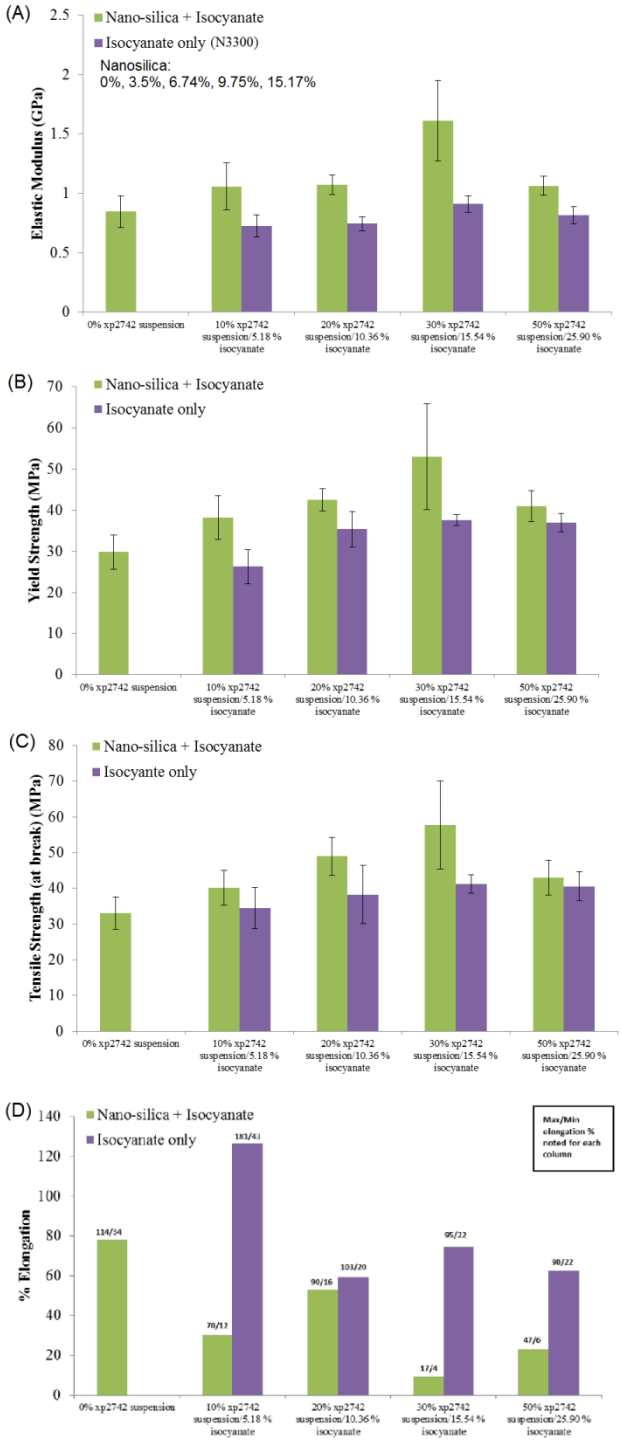

Figure 28: Effect of XP2742 (nanosilica+isocyanate) suspension and N3300 (isocyanate) on tensile properties of PC18M; (A) elastic modulus, (B) yield strength, (C) tensile strength at break, and (D) percent elongation with the numerical values above the bar showing minimum and maximum elongation obtained.